AIChE SYMPOSIUM SERIES
No. 252. Vol. 82
1986

DIFFERENTIAL-INTERFEROMETRIC INVESTIGATION OF CURVED LIQUID FILMS

A. D. Nikolov, P. A. Kralchevsky,
I. B. Ivanov and A. S. Dimitrov ■ Laboratory of Thermodynamics and Physico-chemical Hydrodynamics
Faculty of Chemistry, University of Sofia, 1126 Sofia, Bulgaria

A differential-interferometric method is used for the determination of the film curvature at the top of small air bubbles, attached to a liquid surface. In addition the radius of the contact line and the equatorial bubble radius are measured by direct visual observations. From these data and from the conditions for mechanical equilibrium the film, line and transversal tensions are determined. The measured film and line tensions for bubbles formed in solutions of dodecyl sodium sulfate exhibit a strong dependence on the film curvature and unexpectedly large values of the (negative) line tension. It occurs that the transversal tension effect in the mechanical equilibrium of an attached bubble is of the same order as the disjoining pressure effect.

INTRODUCTION

Differential interferometry is a widespread, powerful and precise method for studying solid surfaces and biological subjects (1-4). The interest in this optical method for investigating fluid surfaces and thin liquid films has grown during the last decade. Zorin (5) has studied a biconcave meniscus in transmitted light. Del Cerro and Jameson (6) and Minqius and Nikolov (7) have applied differential interferometry in reflected light to floating lenses. Recently (8) this method was used for measuring the curvature of the film at the top of small bubbles attached to a liquid surface.

This application of differential interferometry has been stimulated to a large extent by the growing interest in line tension (see e.g. the references in (9). This quantity can affect the occurrence of a number of processes of practical importance, e.g. heterogeneous nucleagion (10,11), flotation of ores (12), droplet coalescence in emulsions (13) and microbial adhestion (14).

Line tension can, in principle, be measured by studying any phenomenon that is affected by it, e.g. from the rate of heterogeneous nucleation (11). This approach requires, however, knowledge (and/or fitting) of several parameters. Therefore, it is better to determine the line tension directly from the conditions for mechanical equilibrium of small particles at another interface.

FILM, LINE and TRANSVERSAL TENSIONS

Let us consider the equilibrium of a bubble (or drop) at a liquid surface - Fig. 1a. All the interfaces are represented in the figure by the corresponding surfaces of tension (see e.g.(15) which satisfy Laplace's equation of capillarity (16) with appropriate boundary conditions. One can describe macroscopically the equilibrium of the film at the top of the bubble with the surrounding phases by considering the film as a single membrane of tension γ which intersects the other two interfaces onto a line called contact line. In our case this line is a circumference of radius r_c - see Fig. 1a. In this approach, called membrane approach, the mechanical equilibrium at each point of the contact line is determined by the balance of four forces (17,9):

$$\underline{\gamma} + \underline{\sigma}_1^{\ell} + \underline{\sigma}_2^{\ell} + \underline{\sigma}_{\kappa} = 0 \qquad (1)$$

Here the vectors $\underline{\gamma}$, $\underline{\sigma}_1^{\ell}$ and $\underline{\sigma}_2^{\ell}$ act tangentially to the film and the two liquid (meniscus) surfaces, and are equal to the film tension γ_{ℓ} and the respective surface tensions σ_1^{ℓ} and σ_2^{ℓ}. The force $\underline{\sigma}_{\kappa}$ is directed toward the center of curvature (18) and is determined by the line tension κ and the radius of curvature, r_c, of the contact line: $|\underline{\sigma}_{\kappa}| = \kappa/r_c$.

The alternative of the membrane approach is to consider the film as a layer of finite thickness, bounded by two surfaces of tensions σ_1^f and σ_2^f - see Fig. 1b. This approach is called detailed (19, 20, 21). There are two contact lines in the detailed approach with line tensions $\tilde{\kappa}_1$ and $\tilde{\kappa}_2$. Each of the lines must be in equilibrium which is determined by the condition

$$\sigma_i^f + \sigma_i^\ell + \underline{\sigma}_i^k + \underline{\tau}_i = 0, \; i = 1,2, \qquad (2)$$

where $|\underline{\sigma}_i^\kappa| = \tilde{\kappa}_i/r_{ci}$ and the vector $\underline{\tau}_i$, called transversal tension, acts on the contact line perpendicularily to the film surfaces inwards (21, 22). In fact the transversal tension accounts for the energy of interaction U^L of the two contact lines, more precisely for flat films $\tau = L^{-1}(\partial U^L/\partial h)$, where h is the film thickness and L is the length of the contact line (21). In this respect it is analogous to the disjoining pressure Π which takes into account the interaction of the two film surfaces (19, 23).

If one takes the horizontal and the vertical projection of the vectorial balance (1) and then solves the two resulting equations with respect to γ and κ, one gets

$$\gamma/\sigma = (\sin\phi_c + \sin\Psi_c)/\sin\theta, \qquad (3)$$

$$\kappa/\sigma = r_c\{\cos\phi_c + \cos\Psi_c - (\sin\phi_c + \sin\Psi_c)\cot\theta\}, \qquad (4)$$

where (for the case of an air bubble) we assumed $\sigma_1^\ell = \sigma_2^\ell \equiv \sigma$, and θ, ϕ_c and Ψ_c are the angles at which the film, bubble and the external meniscus surfaces meet the plane of the contact line - see Fig. 1a. By eliminating θ between (3) and (4) one can obtain a simple (approximate) relation between γ and κ:

$$\kappa/r_c = 2\sigma - \gamma/\cos\alpha, \; \alpha = (\phi_c - \Psi_c)/2. \qquad (5)$$

The contact radius r_c and the equatorial bubble radius R are easily measured by observing the bubble from above. Then the angles ϕ_c and Ψ_c can be calculated from the data for the radii R and r_c using some perturbational formulae, derived in (24), describing the shape of an axisymmetric sessile interface for small values of the capillary number

$$\beta = \rho g b^2/\sigma.$$

Here ρ is the density of the liquid, g is the gravity acceleration and b is the radius of curvature at the bottom of the bubble. The quantities b and β can be calculated from the measured value of R (24):

$$1/b = [1 - \beta/6 + \beta^2(\ell n 2 - 1/6)]/R \qquad (6)$$

using interactions with zeroth approximation $b^{(o)} = R$. With these results for b and β one can calculate ϕ_c as (24):

$$\sin\phi_c = \frac{r_c}{b} - \beta\left(\frac{1}{3}\cot\frac{\phi_c}{2} - \frac{1}{6}\sin 2\phi_c - \frac{1}{2}\sin\phi_c\right) - \beta^2\left[\left(\frac{3}{4} + \frac{1}{2}\cos\phi_c - \frac{2}{9}\sin^2\phi_c - \frac{1}{3}\ell n \sin\frac{\phi_c}{2}\right)\sin\phi_c - \frac{1}{2}\left(1 + \frac{1}{g}\cot^2\frac{\phi_c}{2}\right)\cot\frac{\phi_c}{2}\right] \qquad (7)$$

again using interations with zeroth approximation $\phi_c^{(o)} = \arcsin(r_c/b)$ then Ψ_c can be determined from the equation:

$$\sin\Psi_c = \frac{r_c}{b}\left\{1 + \frac{\beta}{2b}(z_c - h_c)\right\} - \sin\phi_c, \qquad (8)$$

where z_c and h_c are given by (24):

$$z_c = b\{1 + \cos\phi_c + \beta[\tfrac{1}{3}\sin^2\phi_c + \tfrac{2}{3}\ell n \sin\tfrac{\phi_c}{2} - \tfrac{1}{2}(1+\cos\phi_c)]\};$$

$$h_c = r_c \sin\Psi_c \ell n\{4/[\gamma_e(\rho g/\sigma)^{\frac{1}{2}} r_c(1+\cos\Psi_c)]\};$$

$\gamma_e = 1.78\,072\,418\ldots$ is Euler's number. The zeroth approximation to be used in the right-hand side of (8) when calculating Ψ_c by iterations is $h_c = 0$ i.e. $\Psi_c^{(o)} = 0$.

With the calculated values of the angles ϕ_c and Ψ_c one can determine the film tension γ and the line tension κ from Eqs. (3) - (4)

provided that the angle θ is known. Differential interferometry allows the measurement of the radius of curvature of the film R_f (see the next section) and hence, the calculation of θ from

$$\theta = \arcsin(r_c/R_f) \qquad (9)$$

of Fig. 1a.

In addition to the film tension γ and the line tension κ it is interesting to determine experimentally the transversal tension. This can be done with sufficient accuracy from the equation

$$F_b = \pi r_c^2 \Pi - 2\pi r_c \tau_1 \cos\theta, \qquad (10)$$

where for small bubbles $\Pi \approx P_c/2$ ($P_c = 2\gamma/R_f$ is the capillary pressure). Eq. (10) is in fact a force balance: The buoyancy force F_b is counterbalanced by the force $\pi r_c^2 \Pi$ due to the disjoining pressure Π acting over the lower film surface and the force due to the vertical component of τ_1 (see Fig. 1b). The buoyancy force F_b can be calculated by using the value of the angle Ψ_c determined from (8):

$$F_b = 2\pi r_c \sigma \sin\Psi_c. \qquad (11)$$

Determination of the film curvature from the interference pattern

For our measurements of R_f we used the differential - interferometric method of "shearing" with a Epival Interphako Microscope manufactured by Carl Zeiss-Jena (for the construction of the microscope - see Refs. (4) and (25)). The basic principle of the shearing method consists in splitting the original image into two images. The light beams coming from the two images interfere, thus creating a rather complicated interference pattern. An example is shown in Fig. 2, where the shearing distance d = 12.08μm. The upper part of Fig. 3 is a sketch of the cross section (in the plane xOz) of the two images of the reflecting surfaces splitted at a distance d along the x-axis. The plane xOy coincides with the contact line (of radius r_c). The lower part of the figure is a sketch of the resulting interference pattern (cf. Fig.2). One clearly discerns three regions corresponding to the interference of light reflected by the two images of the respective surfaces: (I) meniscus-meniscus (moustaches), (II) meniscus-film (rings) and (III) film-film (streaks). In fact, all fringes are loci of points for which the distance between the reflecting surfaces satisfies the requirement

$$|z_\ell(x,y) - z_r(x,y)| = \ell_n \equiv n\frac{\lambda}{4};\ n=0,1,2,\ldots, \qquad (12)$$

where subscripts "ℓ" and "r" denote left and right hand side images, λ is the light wavelength, and n is the order of interference. The equation of the film shape is

$$z_{\ell,r} = \left(R_f^2 - (x \pm d/2)^2 - y^2\right)^{1/2} - z_o, \qquad (13)$$

where the upper sign refers to the left hand side image, and the lower sign to the right hand side: $z_o = (R_f^2 - r_c^2)^{1/2}$ is the coordinate of the center. Thus, for region III, Equations (12) and (13) lead to

$$x^2/a_n^2 + y^2/b_n^2 = 1 \qquad (14)$$

with

$$a_n = b_n/\varepsilon_n,\ b_n = (R_f^2 - \varepsilon_n^2 \ell_n^2/4)^{1/2},\ \varepsilon_n = (1 + d^2/\ell_n^2)^{1/2}. \qquad (15)$$

Therefore, the streaks are parts of ellipses and the reason why they look like straight lines is the high eccentricity $(1 - 1/\varepsilon_n^2)^{1/2} \approx 1$. Equation (15) allows the calculation of the hat curvature $R_f = \varepsilon_n (a_n^2 + \ell_n^2/4)^{1/2}$ (ℓ_n, a_n and d are known from the experiment).

The visual determination of R_f was performed with complete splitting i.e. with $r_c < d/2$ (d was increased to 24.16μm in this case in order to avoid a gap between photographic and visual measurements). The essence of the method is to record r_c at the moment when the top ring shrinks to a point. From Fig. 4 it follows that at this moment $D_o + Q(d) = \ell_n$, where $Q(d) \equiv Q(x=d)$ is calculated from (24):

$$Q(x) = r_c \left\{ \operatorname{arcosh}\left(\frac{x}{r_c \sin\Psi_c}\right) - \operatorname{arcosh}\left(\frac{1}{\sin\Psi_c}\right) \right\} \cdot \sin\Psi_c$$

Then $R_f = (r_c^2 + D_o^2)/2D_o$.

In order to check the interferometric method we performed some measurements with objects of known curvature (26). We used small sessile water drops on a hydrophobic surface (Teflon) and a mercury drop on glass. The curvature at the top of such a drop can be determined both from the visually measured equatorial drop radius and interferometrically. The interferometrical measurement yields some value b_i for the radius of curvature at the top of such a drop and the independent visual measurement yields another value, b_r, for the same radius. Of course, if there is no systematic error in the interferometric measurements, one must obtain $b_i = b_r$. The data for b_i vs b_r from (26) is shown in Fig.5. One sees that $b_i = b_r$ in the framework of the random error of the measurements but there is not any systematic error in the curvature range studied.

EXPERIMENTS AND DISCUSSION

The experimental method we used to obtain bubbles of different radii is essentially the "shrinking bubble method" of Princen and Mason (27). A relatively large bubble at the liquid surface is allowed to decrease gradually its volume due to the escaping gas through the thin film, and its geometrical parameters are recorded optically as a function of the time.

The experiments were carried out with 0.05% (1.73×10^{-3} kmol/m^3) solutions of dodecyl sodium sulfate (Fisher Scientific, for high performance liquid chromatography) and two concentrations of NaCl (Merck, analytical grade) - 0.25 and 0.32 kmol/m^3. All experiments were carried out in a thermostated room at 22± 0.5°C. The surface tensions of the two solutions used, with 0.25 and o.32 kmol/m^3 NaCl, were 32.4 and 31.7 mN/m(dyn/cm) respectively. The essential part of the measurement cell (the one containing the solution) consists of a glass cylinder of diameter 1 cm and height 1.4 cm whose bottom is an optically plane-parallel glass. The bottom was fixed to the cylinder with glass powder heated at 500°C without using chemical seals. The air bubbles were blown out of a Hamilton syringe. The optical measurements were carried out with a microscope Epival Interphako, Carl Zeiss, Jena. The use of the shearing method was described in the previous section. The values of r_c and R were recorded visually every time when the diameter of the respective circumference became equal to an integar number of scale divisions. At suitably chosen time intervals (100-200 s) the image was splitted and measurements of R_f wer performed either by taking photographs or visually, by counting the number of interference rings.

A major experimental problem is that we need for the calculations the set of values r_c, R and R_f at a given moment, t, whereas some time elapses after the registration of each of these quantities. One possible way to find the required values is by least squares interpolation of the data for $r_c(t)$, R(t) and $R_f(t)$. We interpolated R(t) by the equation

$$R(t) = a_1(t_o-t)^q + a_2(t_o-t)t, \qquad (16)$$

where t_o, q, a_1 and a_2 are constants to be determined by the minimization of the dispersion

$$\phi_1(a_1, a_2, t_o, q) = \sum_i [R(t_i)- R_i]^2. \qquad (17)$$

Here R_i is the measured value of R at the moment t_i and $R(t_i)$ is calculated from Equation (16). Similar interpolation formula were used for $r_c(t)$ and $R_f(t)$.

We have processed in full details only 4 experiments - two for the solution with 0.25 kmol/m^3 NaCl (runs 1a and 1b) and two for 0.32 kmol/m^3 NaCl (runs 2a and 2b). The results are presented in Figs. 6 and 7.

As explained above, when calculating γ and κ we used the data for r_c, R and R_f (at the same moment t), obtained from the interpolation curves $r_c(t)$, R(t) and $R_f(t)$ - see e.g. Equation (16). The error bars in Figs. 6 and 7 denote the standard deviations of $\gamma/2\sigma$ and κ calculated by using the standard deviations of the measured radii r_c, R and R_f with respect to the interpolation curves. The points in the Figs. (calculated from the smooth curves) correspond to the moments, at which R_f was measured, and represent the most probable values of $\gamma/2\sigma$ and κ at those moments.

The most striking features in the behavior of $\gamma/2\sigma$ vs P_c are the large variations of γ (the respective values $\gamma_\infty/2$ for planar films, i.e. for $R_f \to \infty$, taken from Ref. (28), are shown on the ordinate axis of Fig. 6 by arrows) and the fact that at some capillary pressures γ is larger than 2σ (this has not been observed with planar films).

Quite unexpected are the data for κ (Fig. 7) - besides the large values of κ and the variation of κ with r_c, we must point out the change of sign of κ for both solutions of NaCl and to the smaller absolute values of κ for smaller bubbles i.e. for larger r_c^{-1}. There is a tendency of κ to level off for large bubbles ($r_c^{-1} \to 0$), which is more pronounced on the plot κ/σ vs R_f - Fig. 8.

All these findings reveal that (unlike the surface tension and similarly the disjoining pressure) γ and κ are strong functions of the geometrical parameters of the system. This is a new and unexpected result for γ. For the line tension this was predicted on theoretical gounds by many authors (29-33) but has not been observed experimentally.

There have been only a few attempts for experimental determination of the line tension for fluid systems with configuration similar to ours. The authors of Refs. (34) and (35) have studied the same system as ours (bubbles formed from solutions of sodium dodecylsulfate) but their values for κ are different from ours; for example they obtained $\kappa = 0.85$ nN for 0.32 kmol/m^3. The reason for the discrepancy between our and their results lies probably in the fact that they used incomplete experimental information (they did not measure the angle θ) and to make up for this deficiency they erroneously assumed that γ and κ remained constant for all bubble radii.

Navascues and Mederos (11) have determined κ from the nucleation rate of water drops on mercury. They found κ varying from - 0.290 to -0.393 nN for critical radii changing from 20.7 to 25.2nm. These low values of κ should not be surprising in view of the small size of the nuclei.

The only measurements with particle size close to ours were carried out by Torza and Mason (13), who determined κ from the equilibrium configurations of five doublets of emulsion droplets. They obtained five different values for κ (of the order of 10 nN) and attributed these differences to scattering caused by impurities in their system. In fact, a closer inspection of their data reveals that the variation in κ may well be due to geometrical factors. Indeed, their radius of curvature r_{13} of the interface between two droplets corresponds to R_f in our experiments, and if one plots their data for κ vs R_f one obtains, as with our data, a quite good linear dependence - see inset in Fig. 8.

We cannot for the time being completely rule out the possibility that the observed facts are due, at least in part, to non-equilibrium phenomena. Such an effect may be connected with the relatively slow surfactant desorption during the shrinking of the bubble, which can lead to $\sigma_1^\ell \neq \sigma_2^\ell \neq \sigma$ (more precisely $\sigma_1^\ell < \sigma_2^\ell$ - cf. Fig. 1a). But this effect is expected to be more efficient for small bubbles and in this way one hardly could explain the rise of $|\kappa|$ for large bubbles. Besides, such a lowering of σ is unlikely to exist for concentrations above c.m.c. (36). It is more probable that the observed effects are due to some slow irreversible processes, which change the film tension γ(e.g. either condensation of water on the film or gradual change in the film thickness). Because of the connection between γ and κ/r_c (cf. Eq. (5)) this change in γ causes a rise in κ, which counterbalances the alteration in the film tencion (cosd is practially a constant). From a microscopic point of view such a rise in κ may be due to deviations of the transition region (between the film and meniscus) from its equilibrium shape or to local changes of the surface tension in this region - cf. (23). Both effects can have hydrodynamic origin. The definitive explanation of the observed experimental facts requires however additional theoretical and experimental studies which are now under way.

Yet, whatever the origin of these effects might be, we believe to have firmly established that the attachment of small bubbles to a liquid surface gives rise to unexpectedly large line tensions accompanied with corresponding variations of the film tension. Both effects are pronounced functions of the bubble and film radii.

The data for the transversal tension provides additional new information for the equilibrium of an attached bubble. Table I shows how the terms in Eq. (10) vary during the shrinking of a bubble (Run 2a).

It is interesting to note that the buoyancy force F_b is much smaller than the other two terms in (10). In the limiting case of zero gravity (space laboratory) only the disjoining pressure and transversal tension terms will remain in this force balance. The values of the transversal tension τ_1 (last column in Table I) are close to the value 4.77 nN/m, which we calculated from

the data for flat films in Ref. (28) using Eq. (17) from Ref. (21).

In conclusion, these experimental results indicate that the linear effects like the line and transversal tensions could play a much more significant role in the attachment of a fluid particle to another interface than it was believed until now.

REFERENCES

1. Françon, "Progress in Microscopy", Pergamon Press, London, 1961.
2. Françon and S. Mallick, "Polarization Interferometers", Wiley-Interscience, New York, 1971.
3. R. Hoffman and L. Gross, J. Microsc., 91, (1970), 149.
4. H. Beyer, "Theorie and Praxis der Interferenzmikroskopie", Akademische Verlageselschaft, Leipzig, 1974.
5. Z. M. Zorin, Kolloidn. Zh., 39 (1977), 1158.
6. M. C. G. del Cerro and J. Jameson, in "Wetting, Spreading and Adhesion" (J. F. Padday, Ed.), Academic Press, London, 1978.
7. J. Mingins and A. D. Nikolov, Ann. Univ. Sofia (Fac. Chimie), 75 (1981), 3.
8. A. D. Nikolov, P. A. Kralchevsky and I. B. Ivanov, J. Colloid Interface Sci. - to be published.
9. I. B. Ivanov, P. A. Kralchevsky and A. D. Nikolov, J. Colloid Interface Sci. - to be published.
10. R. D. Gretz, Surface Sci., 5 (1966), 239.
11. G. Navascues and L. Mederos, Surface Technol., 17 (1982), 79.
12. A. Scheludko, B. V. Toshev and D. T. Boyadjiev, J. Chem. Soc. Faraday I, 72 (1976), 2815.
13. S. Torza and S. G. Mason, Kolloid Z. u. Z. Polym., 246 (1971), 593.
14. B. A. Pethica, in "Microbial Adhesion to Surfaces", R. C. W. Verkeley, Editor, p. 19, Ellis Horwood, Chichester, U.K.,1980.
15. S. Ono and S. Kondo, in "Handbuch der Physik", Vol. 10, Springer-Verlag, Berlin, 1958.
16. H. M. Princen, in "Surface and Colloid Science" (E. Matijevic and F. R. Eirich, Eds,), Vol. 2, p.1, Wiley, New York, 1969.
17. P. R. Pujado and L. E. Seriven, J. Colloid Interface Sci. 40(1972), 82.
18. V. S. Veselovsky and V. N. Pertzov, Zh. Fiz. Khim., 8 (1936).
19. A. I. Rusanov, "Phase Equilibria and Surface Phenomena", Khimia, Leningrad, 1967 (in Russian); "Phasengleichgewichte und Grenzflächenerscheinungen", Akademie-Verlag, Berlin, 1978.
20. P. A. Kralchevsky and I. B. Ivanov, in "Surfactants in Solutions", K. L. Mittal, Ed., Plenum Press, New York, to be published.
21. P. A. Kralchevsky and I. B. Ivanov, Chem. Phys. Letters, 121 (1985), 111.
22. P. A. Kralchevsky and I. B. Ivanov and A. D. Nikolov, in "Proceedings of the VIth International Conference on Surface Active Substances, Akademie-Verlag, Berlin, to be published.
23. P. A. Kralchevsky and I. B. Ivanov, Chem. Phys. Letters, 121 (1985), 116.
24. P. A. Kralchevsky, I. B. Ivanov and A. D. Nikolov, J. Colloid Interface Sci., to be published.
25. H. Beyer, Jenaer Rdsch., 16 (1971), 82.
26. A. D. Nikolov, A. S. Dimitrov and P. A. Kralchevsky, Optica Acta - submitted for publication.
27. H. M. Princen and S. G. Mason, J. Colloid Sci., 20 (1965), 353.
28. J. A. de Feijter, Thesis, Univ. Utrecht, 1973; see also J. A. de Feijter and A. Vrij, J. Colloid and Interface Sci., 64 (1978), 269.
29. A. I. Rusanov, Kolloidn. Zh., 39 (1977), 704.

30. I. B. Ivanov, B. V. Toshev and B. P. Radoev, in "Wetting, Spreading and Adhesion", J. F. Padday, Editor, p. 37, Academic Press, London, 1978.

31. V. M. Starov and N. V. Churaev, Kolloidn. Zh., 42, 703 (1980).

32. N. V. Churaev, V. M. Starov and B. V. Derjaguin, J. Colloid Interface Sci., 89, 16 (1982).

33. G. Navascues and P. Tarazona, Chem. Phys. Letters, 82, 586 (1981).

34. D. Platikanov, M. Nedyalkov and V. Nasteva, J. Colloid Interface Sci., 75, 620 (1980).

35. A. Scheludko, B. V. Toshev and D. Platikanov, in "The Modern Theory of Capillarity", F. C. Goodrich and A. I. Rusanov, Editors, Akademie Verlag, Berlin, 1981.

36. K. Lunkenheimer-private communication.

Table 1. Bubble parameters during the bubble compression.

TABLE I

R (μm)	r_c (μm)	F_b (μN)	$\pi r_c^2 \Pi$ (μN)	$2\pi r_c \tau_1 \cos\theta$ (μN)	τ_1 (mN/m)
152.7	50.4	0.145	1.66	1.52	4.86
135.9	43.8	0.102	1.41	1.31	4.83
116.2	36.5	0.064	1.14	1.08	4.76
100.3	30.8	0.041	0.945	0.904	4.72
84.5	25.4	0.025	0.764	0.739	4.67
48.5	14.0	0.005	0.402	0.397	4.57
31.5	8.9	0.001	0.252	0.251	4.52

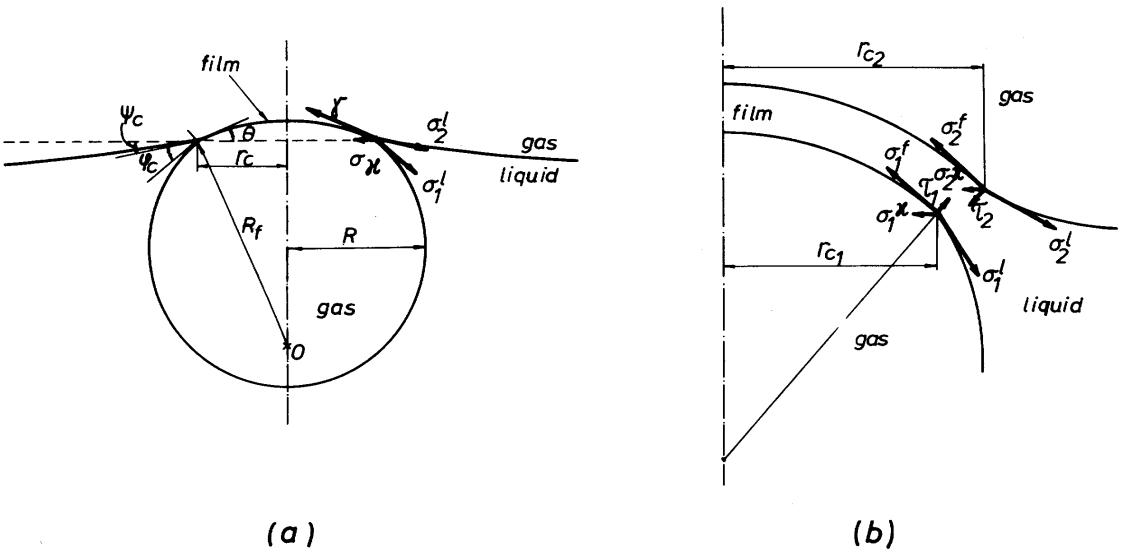

Figure 1. The force balance at each point of the periphery of a spherical thin film in the membrane approach (a) and in the detailed approach (b).

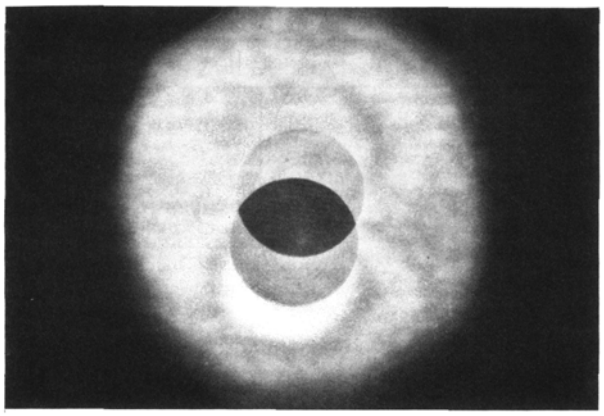

Figure 2. Differential interference pattern in light reflected from a bubble, attached to a deformed air/liquid surface (r_c = 45.4 μm, objective 25x).

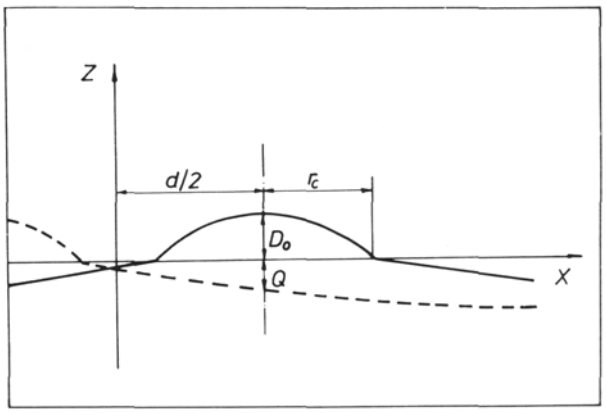

Figure 4. A scheme of the reflecting surfaces in the case of complete splitting (shearing distance $d > 2r_c$).

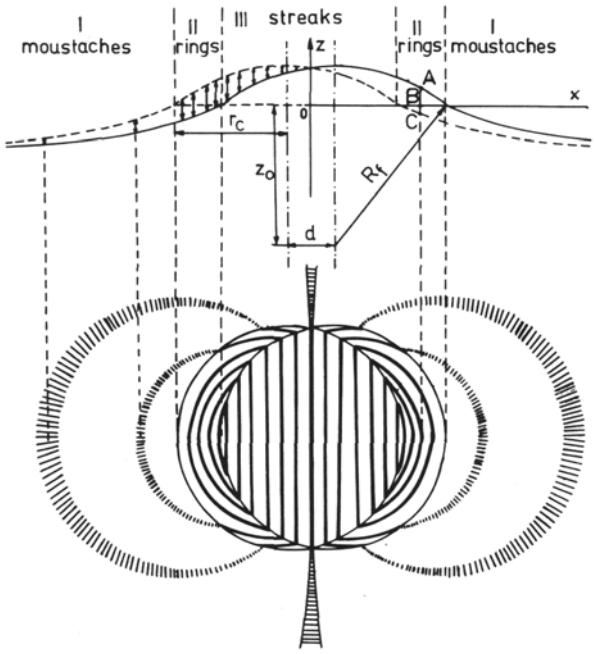

Figure 3. A sketch of the cross section of the reflecting surfaces, shifted at a distance d (upper part) and of the resulting interference pattern (lower part).

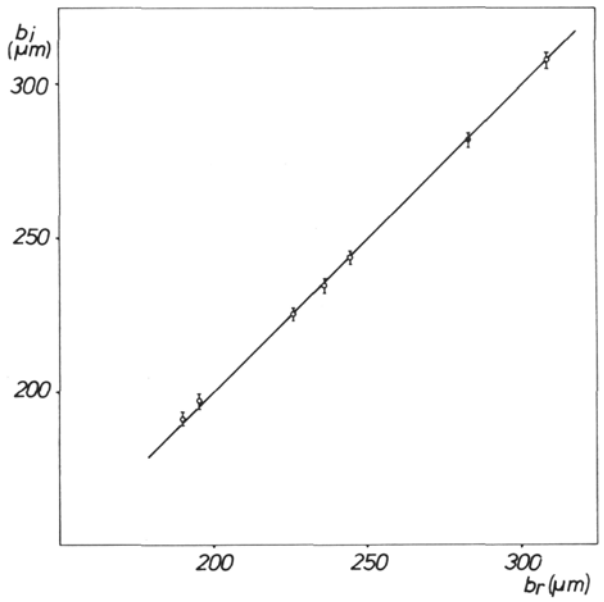

Figure 5. Interferometrically determined radius of curvature b_i vs visually determined value b_r of the same radius for 6 aqueous drops (o) and one mercury drop (●).

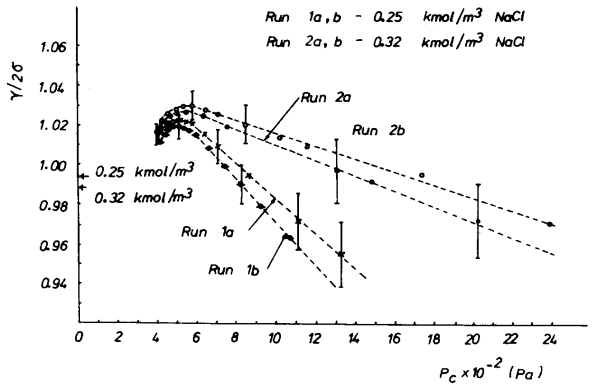

Figure 6. Dimensionless film tension $\gamma/2\sigma$ vs capillary pressure $P_c = 2\gamma/R_f$.

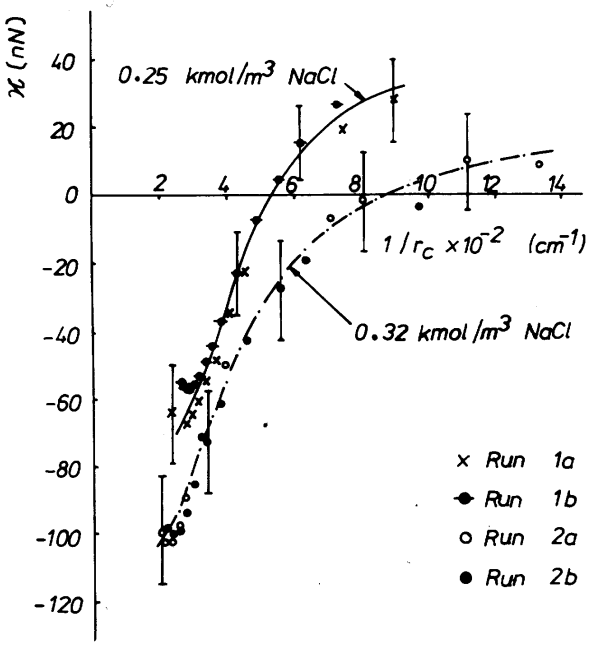

Figure 7. Line tension, κ, vs reciprocal radius r_c^{-1} of the contact line.

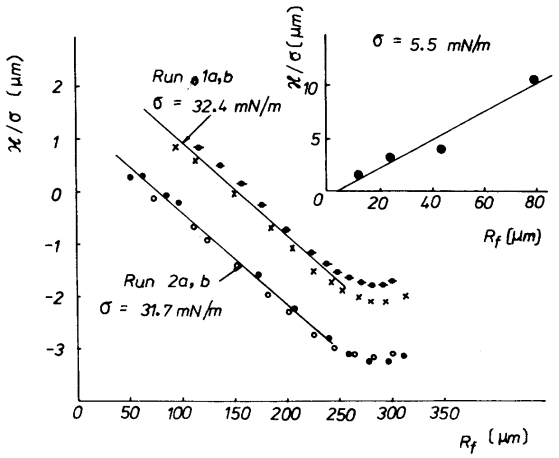

Figure 8. Dependence of κ/σ on R_f (the points correspond to runs: 1a (x), 1b (-●-), 2a (o) and 2b (●). The inset shows the same plot for the data of Torza and Mason (*13*) for doublets of emulsion droplets.